Structural Interpretation of the Zallah Trough and Adjacent Basement Highs in the Western Sirte Basin, Libya: Insights from EGM2008 Geopotential Gravity Data

Isa Mohammed Abuwoden[1]*

[1] Department of Geophysics, Faculty of Science, University of Tripoli, Tripoli, Libya

Corresponding author:

i.abuwoden@uot.edu.ly

ABSTRACT

The Zallah Trough is a structurally significant depocentre in the western Sirte Basin, Libya, whose geometry reflects the interaction between inherited basement fabric and later extensional reactivation. This study develops an integrated structural model of the Zallah Trough and its bounding highs — the Waddan Uplift, Gattar Ridge, Al Qarqaf Arch, and Al Hulayq Ridge — within a window strictly bounded by 17°–18° E and 28°–29° N, using the EGM2008 global geopotential gravity model at a working grid spacing of 1000 m. Bouguer and residual anomaly maps were interpreted jointly with edge-enhancing derivatives (total horizontal gradient, tilt-angle derivative, and analytic signal amplitude), radially averaged power-spectrum depth analysis, three-dimensional Euler deconvolution (structural index 0.0), and a constrained two-dimensional forward-modelled profile (WZG-02) extending from the Waddan Uplift, across the Zallah Trough, to Al Hulayq Ridge.

The Bouguer anomaly field is dominated by a NW–SE-elongated low over the Zallah Trough flanked by positive responses over the surrounding highs. Edge-detection derivatives resolve a dominant NW–SE structural grain with subordinate NE–SW and N–S lineaments, and reveal that the trough itself is internally compartmentalised by at least two discrete sub-depocentres separated by a basement saddle, bounded by two throughgoing marginal faults whose Euler-derived depths deepen systematically from north to south. Power-spectrum analysis yields two well-resolved characteristic depths (7.62 ± 0.22 km, R^2 = 0.987, for a deep source population, and 2.07 ± 0.15 km, R^2 = 0.912, for a shallow population). The forward-modelled profile, calibrated with a sediment density of 2.50 g/cm³ adopted from the median RHOB value of well C5-NC74B and a basement density of 2.7 g/cm³, converges to an RMS misfit of 0.188 mGal after iterative refinement, with a maximum basement depth of 5,050 m beneath the Zallah Trough axis and a minimum of 2,070 m beneath Al Hulayq Ridge; the two largest local misfit zones coincide with independently mapped tilt-derivative zero-crossings at the Waddan Uplift and Al Hulayq Ridge margins, while a residual misfit at the profile's south-eastern end remains unexplained by the mapped lineaments and is attributed to a probable basement density contrast within Al Hulayq Ridge. The results support a fault-controlled, internally segmented horst–graben architecture for the Zallah region and provide a quantitatively constrained regional framework intended to guide, and to be tested against, subsequent seismic and well-based studies.

الملخص

يُعد منخفض زلّة منخفضًا ترسيبيًا ذا أهمية بنيوية في الجزء الغربي من حوض سرت في ليبيا، حيث تعكس هندسته التفاعل بين بنية القاعدة الصخرية الموروثة وعملية إعادة النشاط التمددي اللاحقة. تطوّر هذه الدراسة نموذجًا بنيويًا متكاملًا لمنخفض زلّة والمرتفعات البنيوية المحيطة به وهي: مرتفع ودّان، ومرتفع قطّار، وقوس القرقف، ومرتفع الحليق ضمن نطاق محدد بدقة بين خطي طول 17°–18° شرقًا وخطي عرض 28°–29° شمالًا، وذلك باستخدام نموذج الجهد الجذبي العالمي (EGM2008) بمسافة شبكية قدرها 1000 متر. وقد فُسّرت خرائط شذوذ بوغير والشذوذ المتبقي بصورة مشتركة مع المشتقات المعززة للحواف (التدرج الأفقي الكلي، ومشتق زاوية الميل، وسعة الإشارة التحليلية)، وتحليل أعماق المصادر باستخدام طيف القدرة ذي المتوسط الشعاعي، وتحليل تفكيك أويلر (بمؤشر بنيوي مقداره 0.0)، ونمذجة أمامية ثنائية الأبعاد مقيدة على طول المقطع (WZG-02) الممتد من مرتفع ودّان، عبر منخفض زلّة، وصولًا إلى مرتفع الحليق.

يسيطر على مجال شذوذ بوغير منخفض ممدود باتجاه شمال غرب–جنوب شرق فوق منخفض زلّة، تحيط به استجابات موجبة فوق المرتفعات التكتونية المجاورة. وتوضح مشتقات كشف الحواف اتجاهًا بنيويًا سائدًا باتجاه شمال غرب–جنوب شرق، إلى جانب خطيات ثانوية باتجاه شمال شرق–جنوب غرب وشمال–جنوب، وتكشف أن المنخفض نفسه مقسّم داخليًا إلى مركزين ترسيبيين فرعيين متميزين على الأقل يفصل بينهما سرج قاعدي، ويحدهما صدعان هامشيان مستمران تتزايد أعماقهما المستنتجة من تحليل أويلر بصورة منتظمة من الشمال نحو الجنوب. ويُعطي تحليل طيف القدرة عمقين مميزين ومحددين بدقة 7.62 ± 0.22 كم، بمعامل تحديد $R^2 = 0.987$ لمجموعة المصادر العميقة، و2.07 ± 0.15 كم، بمعامل تحديد $R^2 = 0.912$ لمجموعة المصادر الضحلة.

وقد عُيّرت النمذجة الأمامية للمقطع باستخدام كثافة رسوبية مقدارها 2.50 جم/سم^3، اعتُمدت من قيمة وسيط سجل RHOBللبئر C5-NC74B ، وكثافة قدرها 2.7 جم/سم^3 للقاعدة الصخرية. وقد تقاربت النمذجة إلى جذر متوسط مربع للخطأ (RMS) قدره 0.188 ملي غال بعد التحسين التكراري، مع تسجيل أقصى عمق للقاعدة بلغ 5,050 مترًا أسفل محور

منخفض زلّة، وأدنى عمق بلغ 2,070 مترًا أسفل مرتفع الحليق. وتتوافق مواقع أكبر منطقتين محليتين لعدم المطابقة مكانياً مع موضعي عبور الصفر لمشتق زاوية الميل (TDR)، اللذين حُدِّدا بصورة مستقلة عند هامشي مرتفع ودّان ومرتفع الحليق. أما عدم المطابقة المتبقية عند الطرف الجنوبي الشرقي للمقطع فلا تتوافق مع أي خطية بنيوية مرسومة، ولذلك تُفسَّر بحذر على أنها قد تعكس تغيراً محلياً في كثافة القاعدة الصخرية داخل مرتفع الحليق. وتدعم النتائج بنية هورست–غرابن متحكماً فيها بالصدوع ومجزأة داخلياً في منطقة زلّة، كما توفر إطاراً بنيوياً إقليمياً مقيداً كمياً يهدف إلى توجيه الدراسات الزلزالية ودراسات الآبار اللاحقة، مع ضرورة اختبار هذه النتائج باستخدام تلك البيانات.

Received: 16-02-2026 - Accepted: 24-02-2026 - Published: 02-03-2026

Keywords: Sirte Basin; Zallah Trough; EGM2008 geopotential gravity; Bouguer anomaly; Euler deconvolution; power spectrum; basement depth; horst–graben; tilt derivative; Libya

1. INTRODUCTION

The Sirte Basin is one of Libya's principal sedimentary and hydrocarbon provinces. Its present architecture reflects the superposition of Precambrian–Palaeozoic basement fabric on successive Mesozoic–Cenozoic phases of extension, subsidence, inversion, and fault reactivation (Ahlbrandt, 2001; Anketell, 1996; Goudarzi, 1980). Structural highs and troughs within the basin exert first-order control on accommodation space, sediment thickness, migration pathways, and the location of potential structural traps; mapping the basement configuration and associated fault systems is therefore central to both tectonic reconstruction and petroleum-system evaluation.

The western Sirte Basin comprises a mosaic of troughs, uplifts, arches, and ridges. Around the Zallah Trough, the Waddan Uplift, Gattar Ridge, Al Qarqaf Arch, and Al Hulayq Ridge form major gravity-contrasting domains. Previous gravity and magnetic studies elsewhere in the Sirte Basin —— over the Ajdabiya Trough, the Abu Tumayam Trough, the Gerad Graben, the Raguba Field, and the Zaggut Oil Field (Abdunaser, 2015; El-Batroukh & Zentani, 1980; Eshanibli et al., 2021, 2024, 2025; Omran & Elosta, 2024; Saheel et al., 2010) have consistently shown that potential-field methods can delineate structural trends and estimate characteristic basement depths, but that such interpretations are inherently non-unique and gain substantially in reliability when cross-validated between independent derivative products and constrained by forward modelling.

This study develops a gravity-based structural model for the Zallah Trough and its surrounding highs, strictly within the 17°–18° E, 28°–29° N window, using the EGM2008 global geopotential gravity model gridded at 1000 m spacing. The specific objectives are to: (i) map the regional and residual gravity anomaly fields; (ii) identify probable density boundaries and fault trends using edge-enhancement derivatives, cross-validated against one another; (iii) estimate characteristic source depths using radially averaged power-spectrum analysis and three-dimensional Euler deconvolution; and (iv) test a representative basement geometry along a density-calibrated two-dimensional forward-modelled profile (WZG-02), calibrated against a local well density measurement. The principal contribution is a multi-method, internally cross-validated structural interpretation of the Zallah region, together with an explicit, quantitative account of where the interpretation is well constrained and where it remains uncertain.

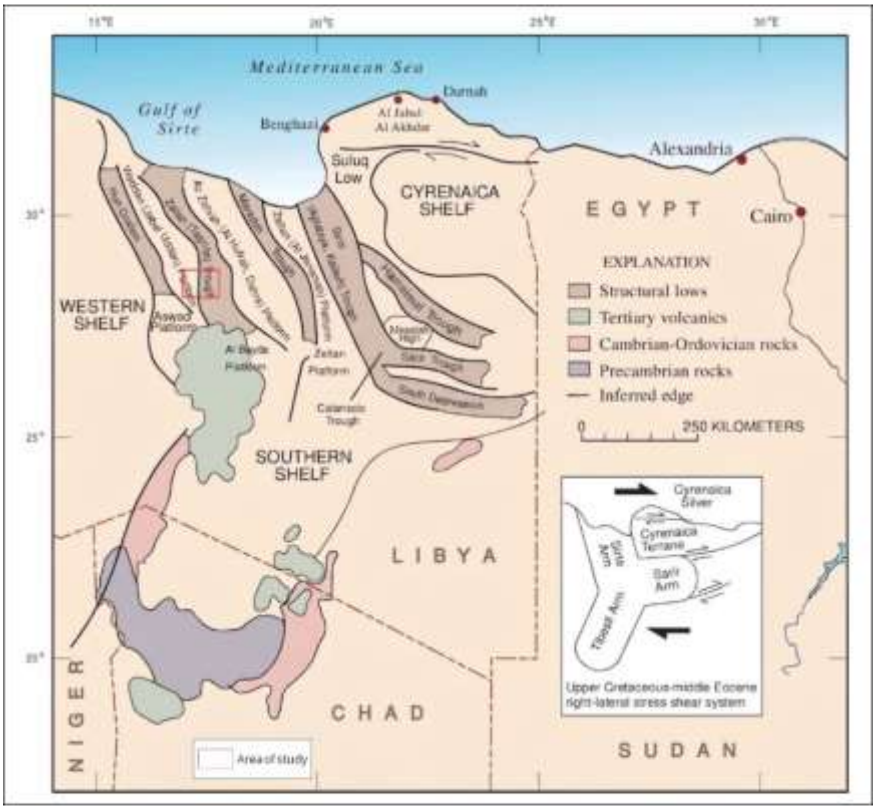

Figure 1. Location and geological setting of the study area. (a) Regional structural elements of the Sirte Basin, Libya, showing the location of the Zallah Trough study area (17°–18° E, 28°–29° N, red box) within the broader basin framework (modified from Ambrose, 2000); troughs/grabens and platforms/horsts are used synonymously in the regional literature, and fault barbs indicate the direction of relative fault movement. (b) Detailed structural map of the Zallah region showing the Zallah Trough, adjacent structural highs (Waddan Uplift, Gattar Ridge, Al Qarqaf Arch, Al Hulayq Ridge), and major mapped fault trends.

2. GEOLOGICAL AND TECTONIC SETTING

The study area occupies the western Sirte Basin, strictly within 17°–18° E and 28°–29° N, bounded by the Al Qarqaf Arch, Waddan Uplift, Gattar Ridge, and Al Hulayq Ridge. Within this framework, the Al Qarqaf Arch and Al Hulayq Ridge are interpreted as basement-involved highs to the southwest and southeast respectively, the Gattar Ridge forms a basement high to the northeast, and the Zallah Trough occupies the intervening sediment-filled low. The gravity response of these domains reflects the contrast between relatively shallow, dense crystalline basement on the highs (basement density 2.7 g/cm³, this study) and a thicker, lower-density sedimentary succession within the trough (2.50 g/cm³, this study).

The regional structural grain is dominated by a NW–SE orientation, accompanied by subordinate NE–SW and N–S lineaments, consistent with inherited basement fabric reactivated during Cretaceous extension and subsequent tectonic phases. A gravity lineament is not necessarily a single discrete fault: it may represent a lithological boundary, a basement step, or a lateral change in sediment thickness. This distinction is maintained throughout the interpretation, and mapped lineaments are treated as probable fault-related or basement-boundary features rather than as directly observed fault planes, except where corroborated by convergent evidence from multiple independent derivative products, as documented in Section 4.

Gravity highs are interpreted, cautiously, as areas of shallower or relatively denser basement, whereas gravity lows are associated with deeper basement and thicker sedimentary accumulation. Such basement-controlled depocentres and structural highs can influence accommodation space, facies distribution, trap development, and migration pathways, and are therefore relevant to petroleum-system analysis in a general, regional sense. Gravity anomalies alone, however, cannot demonstrate the presence of a working petroleum system; any petroleum-system inference drawn from the present analysis must be regarded as regional and conceptual until it is constrained by seismic data, additional well information, and geochemical evidence. All statements in this manuscript regarding structure and petroleum context refer exclusively to features within the 17°–18° E, 28°–29° N window.

3. DATA AND METHODS

The analysis uses the EGM2008 global geopotential gravity model in the WGS 84 reference system, gridded at a spacing of 1000 m across a window bounded strictly by 17°–18° E and 28°–29° N. As a global satellite-derived model, EGM2008 resolves regional- to intermediate-wavelength gravity signal but has inherent resolution limits at short wavelengths; this constraint is addressed quantitatively in Section 3.4 and treated as a first-order limitation throughout the interpretation (Section 6). The overall processing and interpretation workflow is summarised in Figure 2

3.1 Edge-enhancement derivatives

The total horizontal gradient (THG) of the gravity field g was used to enhance the lateral boundaries of density contrasts:

$$THG(x,y) = [(\partial g/\partial x)^2 + (\partial g/\partial y)^2]^{1/2} \quad (1)$$

where $\partial g/\partial x$ and $\partial g/\partial y$ are the horizontal derivatives of the gravity field in the x (easting) and y (northing) directions. THG maxima mark the approximate lateral position of density boundaries, though their position may be displaced by source depth and by interference between neighbouring sources **(Eshaghzadeh, 2015)**

The tilt-angle derivative (TDR), which is independent of anomaly amplitude and therefore complements THG, was computed as:

$$TDR(x,y) = \arctan[(\partial g/\partial z) / THG(x,y)] \quad (2)$$

where $\partial g/\partial z$ is the vertical derivative of the gravity field. TDR is positive over the source, passes through zero approximately over its edge, and is negative off the source; the TDR zero-contour was used as a primary, amplitude-independent indicator of probable structural boundaries **(Miller & Singh, 1994)**.

The analytic signal amplitude (AS), independent of the sign of the density contrast, was computed as:

$$AS(x,y) = [(\partial g/\partial x)^2 + (\partial g/\partial y)^2 + (\partial g/\partial z)^2]^{1/2} \quad (3)$$

AS peaks were used as a third, independent line of evidence for source-edge location, particularly to corroborate boundaries identified from THG and TDR (Verduzco et al., 2004).

3.2 Radially averaged power spectrum

The radially averaged power spectrum of the gravity field was used to estimate characteristic depths to ensembles of gravity sources, following the standard relationship between the logarithm of spectral power and wavenumber (Blakely, 1996):

$$\ln P(k) = C - 4\pi hk \quad (4)$$

where P(k) is the radially averaged power at wavenumber k (cycles per grid unit), C is a constant, and h is the mean depth to the top of the source ensemble contributing to that wavenumber band. Linear segments were fitted by least-squares regression to distinguish deeper and shallower source populations, and depth was recovered from the fitted slope as h = −slope / 4π, with uncertainty propagated from the standard error of the regression slope.

3.3 Three-dimensional Euler deconvolution

Three-dimensional Euler deconvolution was applied to the residual gravity grid (RES.grd) to estimate source locations and depths, based on Euler's homogeneity equation (Reid et al., 1990):

$$(x - x_0)(\partial g/\partial x) + (y - y_0)(\partial g/\partial y) + (z - z_0)(\partial g/\partial z) = N(B - g) \quad (5)$$

where (x_0, y_0, z_0) is the source location to be solved for, (x, y, z) is the observation point, N is the structural index (a measure of the rate of decay of the field with distance from the source), B is the regional background level, and g is the observed field value at (x, y, z). A structural index of N = 0 was selected because the Euler deconvolution was intended to delineate density-contrast edges and contact-type structural boundaries rather than estimate the geometry of cylindrical or spherical bodies. Processing was performed with a grid spacing of 1000 m and a moving window of 20 × 20 cells (20,000 m × 20,000 m). The maximum percentage depth tolerance (15%) and the maximum distance-to-accept criterion (10,000 m) were tuned iteratively until the retained solutions formed spatially coherent clusters consistent with the independently mapped THG and TDR lineaments; solutions failing this joint coherence criterion were rejected as noise. Only a single structural index

(N = 0.0) was tested in this study; a formal sensitivity test across alternative structural indices was not performed and is recommended as future work (Section 6).

3.4 Two-dimensional forward modelling

Two-dimensional forward gravity modelling was performed using GM-SYS Profile, which implements the Talwani polygon-based forward-modelling algorithm. A single representative profile, WZG-02, was modelled across the study area, extending from the Waddan Uplift in the northwest, across the Zallah Trough, to Al Hulayq Ridge in the southeast, over a total length of 127,903 m. The forward model consists of a sedimentary cover overlying a basement complex. The basement density of 2.7 g/cm³ was adopted as a representative modelling value; this value is close to the 2.67 g/cm³ Bouguer reduction density used for regional potential-field processing over the Zelten Platform in the Sirte Basin (Eshanibli et al., 2020). Well C5-NC74B provided the primary density reference for the logged sedimentary interval. Quality control was performed using the DRHO correction log. The DRHO values remained close to zero throughout the logged interval, supporting the reliability of the RHOB measurements used for density estimation. The RHOB log yielded a mean density of 2.52 g/cm³ and a median of 2.50 g/cm³ (n = 2,120 readings). The value of 2.50 g/cm³ was adopted directly as the sediment density in the forward model, consistent with the median RHOB value, and was held constant with depth as a modelling simplification.

Three candidate wells (C4-NC74B, C5-NC74B, C6-NC74B; operator: Zueitina Oil Company), belonging to the Safsaf field — one of several petroleum fields located within the broader Zallah region — were identified within the study window and evaluated as potential density-calibration sources (Table 1). The three wells are located within approximately 1.3 km of one another and reach comparable total depths (2,255–2,304 m), consistent with penetrating the same stratigraphic sequence. Well C5-NC74B was selected as the calibration well on two independent grounds: (i) it is the deepest of the three (total depth 7,560 ft / 2,304.3 m), and (ii) its surface location (28°38′56.664″ N, 17°20′35.823″ E) falls within the deepest of the internal closed minima resolved along the Zallah Trough axis in Sections 4.1–4.3, making it geographically, and not only numerically, the most representative of the three for calibrating basin-axis sediment density. Well C5-NC74B is operated as an injection well; because the bulk-density (RHOB) log reflects a physical rock property measured during drilling, independent of the well's subsequent operational role, this does not affect the reliability of the density value derived from it.

Table 1. Candidate calibration wells identified within the study window.

Well	Field / Operator	Location (Lat, Lon)	Total depth
C4-NC74B	Safsaf / Zueitina	28°39′29.774″N / 17°20′07.831″E	7,450 ft (2,271.8 m)
C5-NC74B (selected)	Safsaf / Zueitina	28°38′56.664″N / 17°20′35.823″E	7,560 ft (2,304.3 m)
C6-NC74B	Safsaf / Zueitina	28°38′57.50″N / 17°19′58.91″E	7,400 ft (2,255.5 m)

The adopted sediment density of 2.50 g/cm³ was held constant with depth as a modelling simplification. Because well C5-NC74B does not reach the interpreted basement, the RHOB calibration constrains the sedimentary density but does not directly constrain the deeper basement geometry. Compaction-related density increase and other depth-dependent variations are therefore not represented in the current model.

The model was refined iteratively by adjusting the depth of the basement interface at individual nodes until the calculated gravity response matched the observed residual profile to an acceptable tolerance, reducing the root-mean-square (RMS) misfit from an initial value of 0.28 mGal to a final value of 0.188 mGal. Node adjustments were accepted only where they coincided with independently mapped structural boundaries (Section 4.3–4.4); adjustments not supported by convergent edge-detection evidence were treated with caution and are flagged accordingly in Section 5.

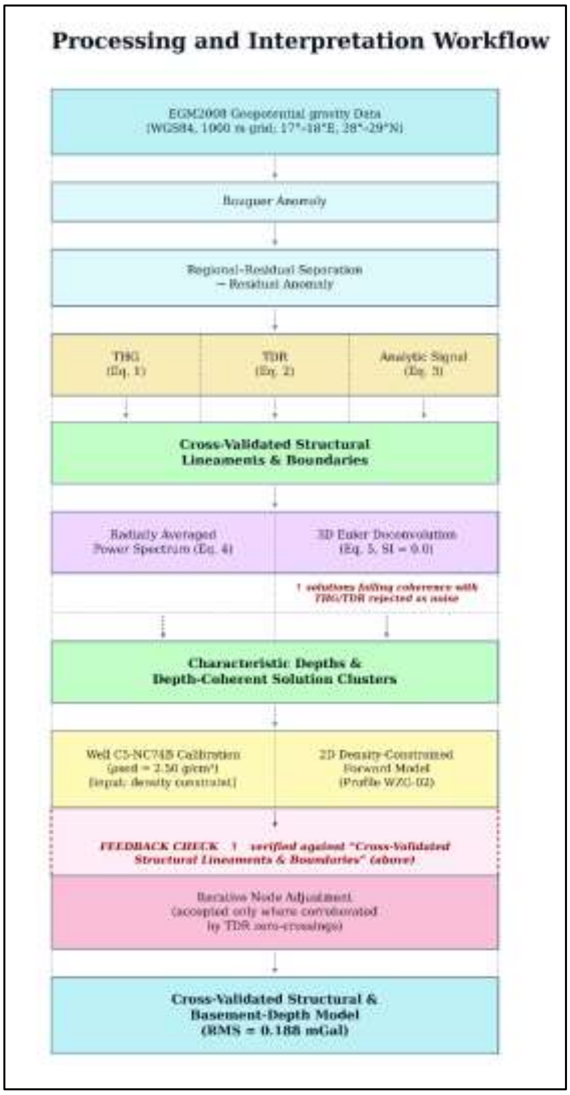

Note: Grey/navy dotted arrows indicate the primary processing sequence. Red and pink annotations and boxes indicate cross-validation and feedback checks: (1) Euler solutions inconsistent with the THG/TDR lineaments were rejected as noise (Section 3.3); and (2) the forward-model results were checked against the cross-validated structural lineaments and boundaries, while basement-interface node adjustments were accepted only where further corroborated by independently mapped TDR zero-crossings (Section 3.4).

Figure 2. Processing and interpretation workflow, from the EGM2008 regional gravity field through Bouguer and residual anomaly separation, three independent edge-detection derivatives (THG, TDR, and analytic signal), parallel depth estimation (power spectrum and 3D Euler deconvolution), the density-calibrated 2D forward model along profile WZG-02, and the final cross-validated structural and basement-depth synthesis. Red and pink annotations and boxes indicate cross-validation and feedback checks: (1) Euler solutions inconsistent with the THG/TDR lineaments were rejected as noise (Section 3.3); and (2) the forward-model results were checked against the cross-validated structural lineaments and boundaries, while basement-interface node adjustments were accepted only where further corroborated by independently mapped TDR zero-crossings (Section 3.4).

4. RESULTS

4.1 Bouguer gravity anomaly

The Bouguer anomaly (Figure 3) field ranges from approximately −33.4 to +9 mGal across the study window. The clearest, most tightly closed high in the entire map coincides with Al Qarqaf Arch, bounded by steep, closely spaced contours indicative of a sharp lateral density contrast; Gattar Ridge forms a broad positive zone in the northeast that does not close within the window, indicating that its true culmination may lie partly outside the study area. Waddan Uplift, at the northwestern margin of the window, is expressed only weakly (values near 0 to −8 mGal), suggesting that only its flank, rather than its core, falls within the mapped window. The Zallah Trough forms a NW–SE-elongated low that is not a single simple depocentre: at least two discrete closed minima are resolved along its axis, separated by a subtle basement saddle, together with a third, more tightly closed and steeper-sided low farther south. A separate deep low occurs at the extreme southeastern corner of the window, offset from and more N–S/NE–SW-oriented than the main trough axis; because this feature touches the window edge it cannot be fully characterised and may be affected by edge truncation of the EGM2008 extraction.

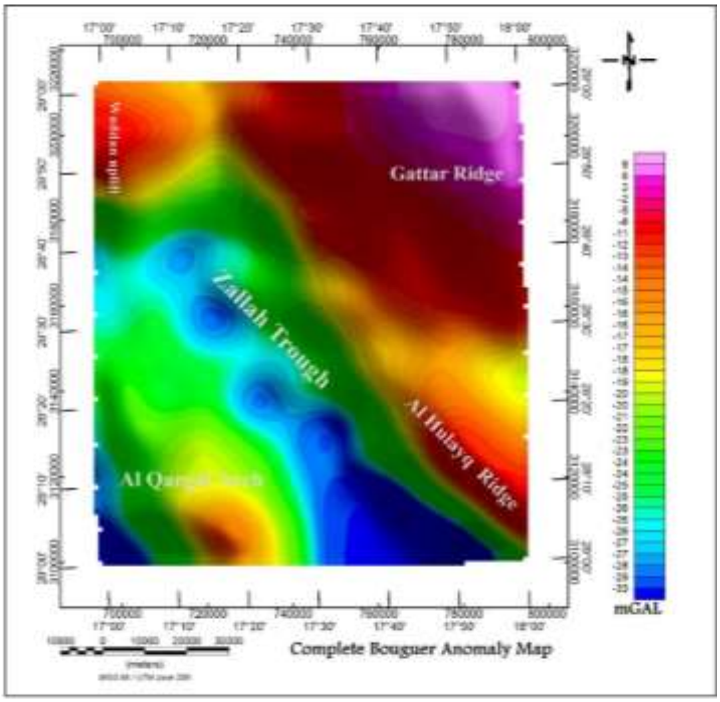

Figure 3. Bouguer gravity anomaly map of the study area (mGal), EGM2008, 1000 m grid spacing. The NW–SE-elongated low corresponds to the Zallah Trough, internally segmented into at least two closed minima; the flanking highs correspond to the Waddan Uplift, Gattar Ridge, Al Hulayq Ridge, and Al Qarqaf Arch

4.2 Residual gravity anomaly

The first-order surface was selected because the study focuses on delineating local and medium-wavelength structural features associated with the Zallah Trough and adjacent basement highs. As a sensitivity check, a second-order polynomial trend surface was also tested. It produced residual-anomaly patterns nearly identical to those obtained with the first-order surface, including the locations, amplitudes, and orientations of the principal anomalies. The first-order result was therefore retained for the subsequent interpretation. The resulting residual anomaly map is shown in Figure 4.

The residual anomaly map sharpens the expression of the individual structural domains after removal of the long-wavelength regional field. The two internal closed minima identified in the Bouguer field are reproduced at consistent locations in the residual field, raising confidence that they represent genuine sub-basin compartments rather than gridding artefacts. A previously unremarked, spatially confined low is also resolved within the otherwise positive expression of Al Hulayq Ridge, suggesting a local sedimentary pocket or fault sliver cutting the ridge itself. The deep low in the southeastern corner persists at comparable amplitude in the residual field, reinforcing that it is a genuine, if incompletely resolved, feature rather than a purely regional-field artefact.

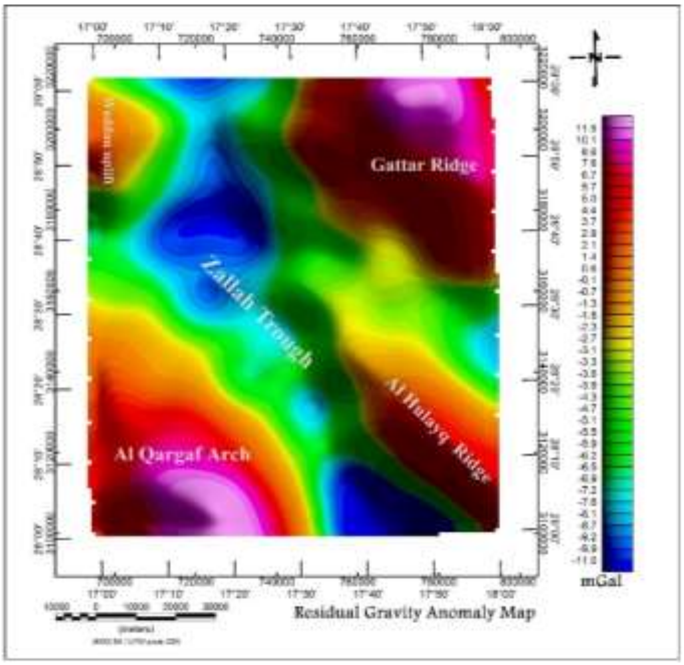

Figure 4. Residual gravity anomaly map of the Zallah region (17°–18° E, 28°–29° N), mGal. The Zallah Trough is resolved as an internally segmented low bounded by the Waddan Uplift, Gattar Ridge, Al Qarqaf Arch, and Al Hulayq Ridge; a local low within Al Hulayq Ridge and a separate deep low in the southeastern corner are also identified.

4.3 Edge detection: THG, TDR, and analytic signal

The THG map (Figure 5) shows the highest gradient magnitudes along an extended, laterally continuous zone bounding Al Qarqaf Arch on its northern side, and along a second zone separating the Zallah Trough from Al Hulayq Ridge. A prominent, near-equant (non-elongate) zone of high THG occurs south of the main trough, distinct in shape from the elongate linear zones elsewhere, suggesting a spatially confined source rather than a simple planar fault at that location.

The TDR map, overlaid with its zero-contour (Figure 6), confirms both bounding trends as laterally continuous, and additionally resolves a small, fully closed zero-contour loop isolated from the regional lineament pattern, consistent with a spatially confined local source. Along a representative profile crossing the trough (WZG-02; Section 4.5), the TDR field crosses zero at two locations: at a cumulative distance of approximately 16,886 m from the profile origin (the Waddan Uplift / Zallah Trough boundary) and at approximately 61,047 m (the Zallah Trough / Al Hulayq Ridge boundary).

The combined THG–TDR overlay (Figure 7) and the analytic signal amplitude map (Figure 8) were used jointly to distinguish major, laterally persistent lineaments from shorter, more localised boundaries, following continuity, amplitude, and mutual agreement between the three derivative products (Eshaghzadeh, 2015; Miller & Singh, 1994; Verduzco et al., 2004). The two internal closed minima identified in Section 4.1–4.2 coincide, in both maps, with compact zones of elevated analytic signal amplitude, independent of the sign of the underlying density contrast — a third, independent line of evidence that these are genuine, discrete basement compartments. The near-surface expression of the trough's deepest zone in the analytic signal map is broader and more equant than its elongate NW–SE expression in the Bouguer field, suggesting that the basin geometry may not be uniform with depth; this is discussed further in Section 5.

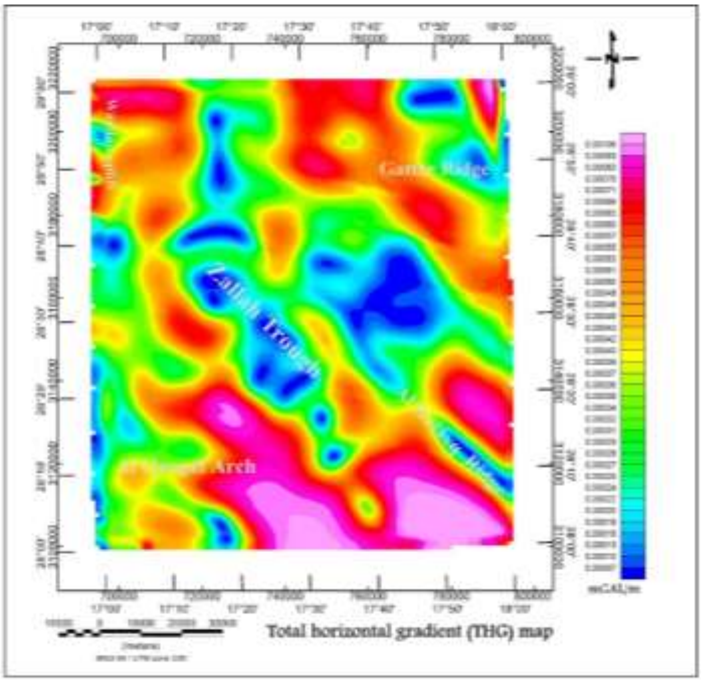

Figure 5. Total horizontal gradient (THG) map, mGal/m, showing the principal density-contrast boundaries bounding the Zallah Trough and the near-equant high-gradient zone south of the trough.

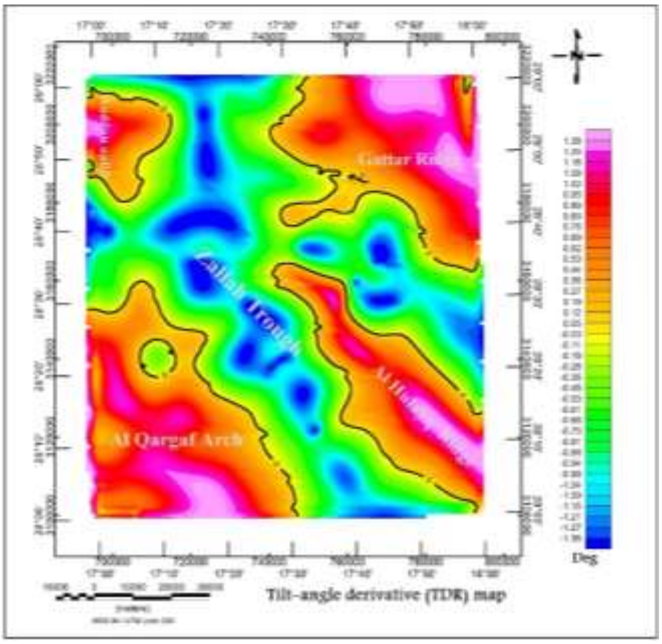

Figure 6. Tilt-angle derivative (TDR) map, degrees, with the zero-contour overlaid, marking the inferred lateral edges of density-contrast sources, including an isolated closed loop indicative of a spatially confined local source.

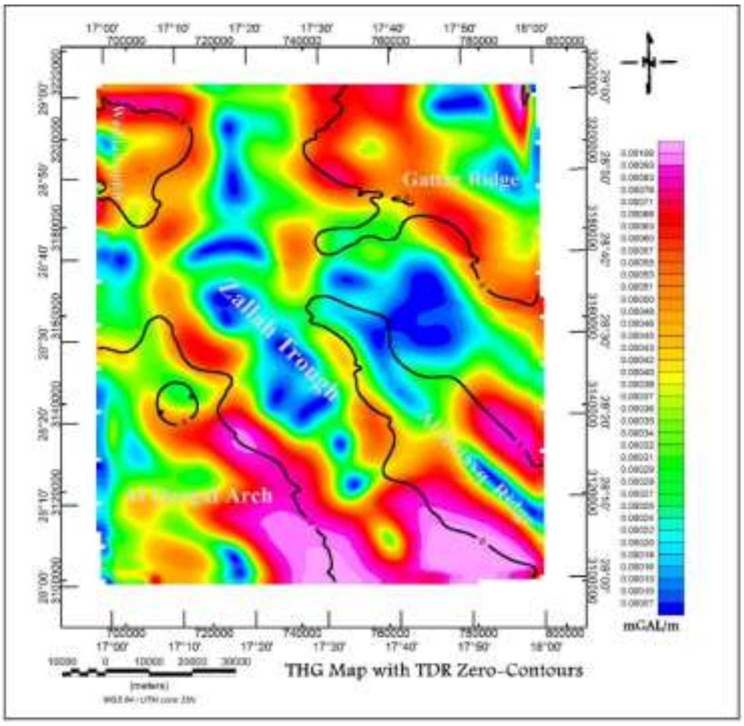

Figure 7. Total horizontal gradient map overlaid with tilt-derivative zero-contour lines, used to cross-validate major structural lineaments bounding the Zallah Trough.

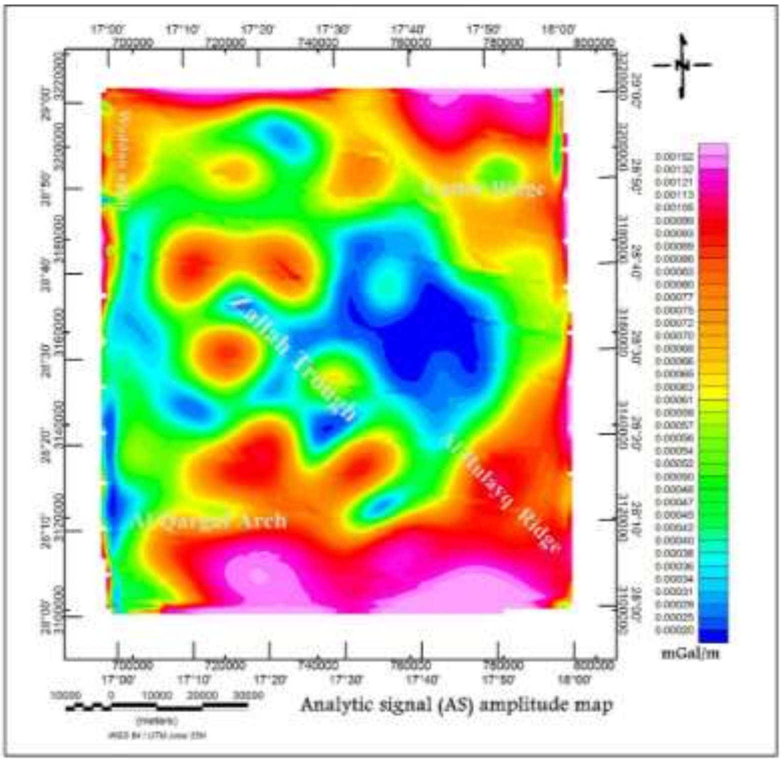

Figure 8. Analytic signal (AS) amplitude map, mGal/m, showing amplitude highs that help corroborate the boundaries and internal compartmentalisation of the Zallah Trough independently of the THG and TDR results.

4.4 Depth estimation

The radially averaged power spectrum (Figure 9) resolves two linear segments with distinct slopes. A deep source population, fitted over the wavenumber range 0.0079–0.1350 cycles per grid unit (18 points), yields a depth of 7.62 ± 0.22 km (R^2 = 0.987), plausibly associated with the regional basement surface beneath the Zallah Trough and adjacent highs. A shallow source population, fitted over the wavenumber range 0.1905–0.3492 cycles per grid unit (21 points), yields a depth of 2.07 ± 0.15 km (R^2 = 0.912), consistent with shallower intrasedimentary or near-surface density contrasts. The high-wavenumber tail of the spectrum (beyond approximately 0.40 cycles per grid unit) flattens and is interpreted as the noise floor associated with the resolution limit of the EGM2008 model at 1000 m grid spacing; it was excluded from both regression fits.

Table 2. Power-spectrum results.

Source population	Wavenumber range (cyc/unit)	n	Estimated depth (km)	R^2
Deep source	**0.0079 – 0.1350**	**18**	**7.62 ± 0.22**	**0.987**
Shallow source	**0.1905 – 0.3492**	**21**	**2.07 ± 0.15**	**0.912**

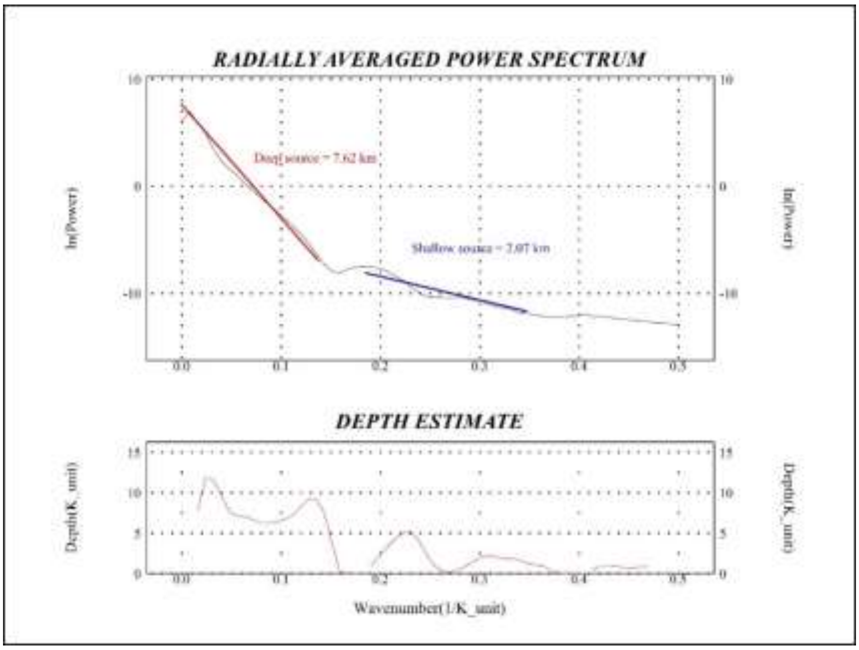

Figure 9. Radially averaged power spectrum [ln P(k) vs wavenumber k] with fitted linear segments for the deep (7.62 km) and shallow (2.07 km) source populations, and the corresponding local depth-estimate curve.

Three-dimensional Euler deconvolution (Figure 10a), applied to the residual gravity grid with structural index N = 0.0, a 1000 m grid spacing, a 20 × 20-cell window, a maximum depth tolerance of 15%, and a maximum accept-distance of 10,000 m, yields spatially coherent solution clusters along both margins of the Zallah Trough, consistent with the independently mapped THG and TDR lineaments (Section 4.3). Direct overlay of the retained solutions on the TDR zero-contour (Figure 10b) confirms this spatial coherence visually, with solution clusters closely tracking the zero-crossings along both margins. Along both margins, the retained solutions show a systematic deepening from north to south, from depths of less than 1,500 m in the north to depths of approximately 8,000–8,500 m in the south, with local solutions exceeding 8,500 m, consistent with both bounding faults being dipping structures rather than vertical. The zone where the two marginal fault trends converge in the south, at the southern end of the Zallah Trough, corresponds to the deepest and most concentrated cluster of solutions in the entire dataset (with depths exceeding 7,000 m and locally more than 8,500 m), reinterpreted here as a fault-intersection zone rather than a shallow basement saddle, based on this depth evidence.

Table 3. Euler deconvolution parameters.

Parameter	Value used
Input grid	RES.grd (residual gravity)
Structural index (N)	0.0
Grid spacing	1000 m
Window size	20 × 20 cells (20,000 m × 20,000 m)
Max. % depth tolerance	15% (tuned iteratively)
Max. distance to accept	10,000 m (tuned iteratively)
Depth range retained	< 1,500 m to > 8,500 m
Cluster acceptance criterion	Spatial coherence and agreement with independently mapped THG/TDR lineaments
Sensitivity test across N	Not performed (single N = 0.0 run); recommended as future work

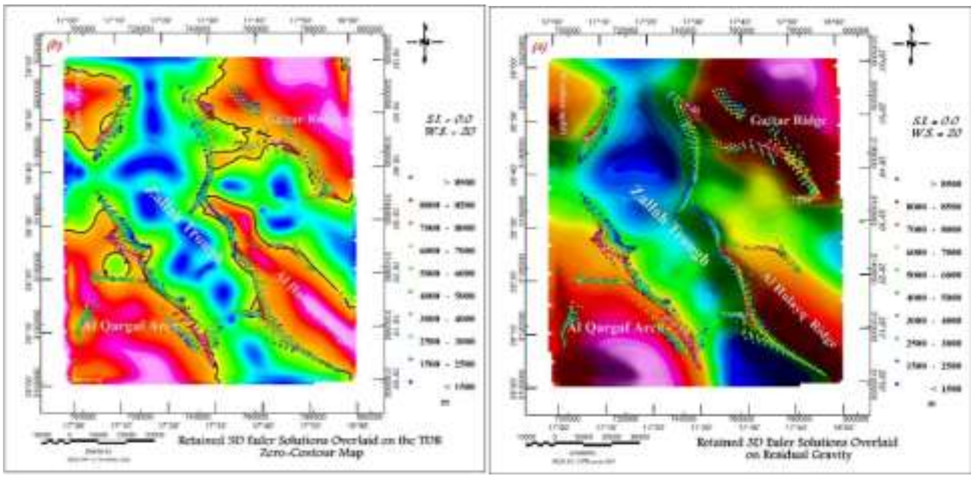

Figure 10. Three-dimensional Euler-deconvolution solutions, computed using a structural index of N = 0.0 and colour-coded by estimated depth (m), overlaid on (a) the residual-gravity field and (b) the TDR map with the zero-contour superimposed. The solutions form coherent clusters along the trough margins and deepen systematically from north to south.

4.5 Two-dimensional forward model — profile WZG-02

Profile WZG-02 (127,903 m long) extends from within the flank of the Waddan Uplift in the northwest, across the Zallah Trough, to within Al Hulayq Ridge in the southeast (Figure 11a). The forward model, calibrated with a sediment density of 2.50 g/cm³ adopted from the median RHOB value of well C5-NC74B and a basement density of 2.7 g/cm³, converges to an RMS misfit of 0.188 mGal, which was reduced from an initial unadjusted misfit of 0.28 mGal through iterative adjustment of the basement-interface node depths.

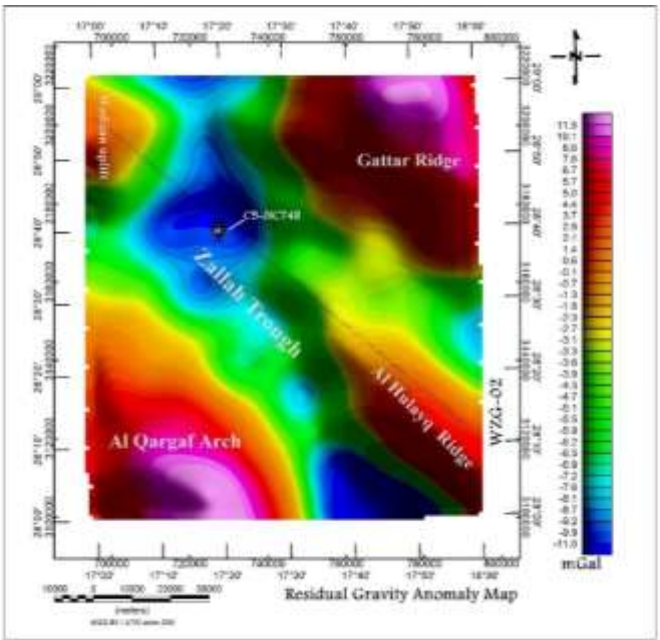

Figure 11a. Residual gravity anomaly map of the Zallah region showing the location and orientation of profile WZG-02, extending from the Waddan Uplift (northwest) across the Zallah Trough to Al Hulayq Ridge (southeast).

The surface location of calibration well C5-NC74B projects onto the profile at approximately 25–30% of its total length from the Waddan Uplift end, placing it within the deepest of the internal closed minima identified along the Zallah Trough axis in Sections 4.1–4.3. This provides an independent, purely geographic corroboration — separate from the density calibration itself — that the closed minima resolved from the Bouguer, residual, and analytic signal fields correspond to a genuine, drillable sub-basin rather than a processing artefact. The well's total depth (2,304 m) is markedly shallower than the modelled basement at this location, illustrating directly that the calibration constrains only the upper part of the modelled sedimentary section (Section 3.4; Figure 11b). The resulting basement geometry deepens from the northwestern end of the profile to a maximum depth of 5,050 m beneath the Zallah Trough axis, then shallows to a minimum depth of 2,070 m beneath Al Hulayq Ridge at the southeastern end. The interface is not a simple smooth sag but shows a stepped geometry, consistent with the fault-bounded, horst–graben architecture inferred from Sections 4.1–4.4. The two principal steps in the modelled interface — near cumulative distance 16,886 m and 61,047 m along the profile — coincide precisely with the two TDR zero-crossings identified in Section 4.3, providing direct, quantitative corroboration that these steps represent genuine basement faults rather than modelling artefacts.

A residual local misfit, the largest along the entire profile (up to 0.51 mGal), occurs at the profile's southeastern end (approximately 117,567–127,903 m), entirely within Al Hulayq Ridge. This zone is not associated with any TDR zero-crossing or other independently mapped lineament, and is therefore not attributed to an unmodelled fault; it is instead attributed, provisionally, to a basement density within Al Hulayq Ridge that departs from the uniform 2.7 g/cm³ assumed across the model, a limitation discussed further in Section 6. It is noted that the modelled maximum depth (5,050 m) is substantially shallower than both the power-spectrum deep-source depth (7.62 km, Section 4.4) and the deepest Euler solutions in the fault-intersection zone (>8,500 m, Section 4.4); this is not a contradiction, since profile WZG-02 does not cross the fault-intersection zone identified at the southern convergence of the two marginal faults, and the power-spectrum depth represents a window-averaged regional estimate rather than a value local to this specific profile.

Table 4. Summary of the WZG-02 forward-model results.

Parameter	Value
Profile length	127,903 m
Profile orientation	NW (Waddan Uplift) to SE (Al Hulayq Ridge)
Sediment density	2.50 g/cm^3 (median RHOB from well C5-NC74B; TD 2,304 m < modelled basement)
Basement density	2.7 g/cm^3
Maximum basement depth	5,050 m (beneath Zallah Trough axis)
Minimum basement depth	2,070 m (beneath Al Hulayq Ridge)
Final RMS misfit	0.188 mGal (initial unadjusted misfit: 0.28 mGal)
Principal corroborated fault steps	≈16,886 m and ≈61,047 m (coincide with TDR zero-crossings)
Unresolved local misfit	≈117,567–127,903 m (up to 0.51 mGal; not linked to a mapped lineament)

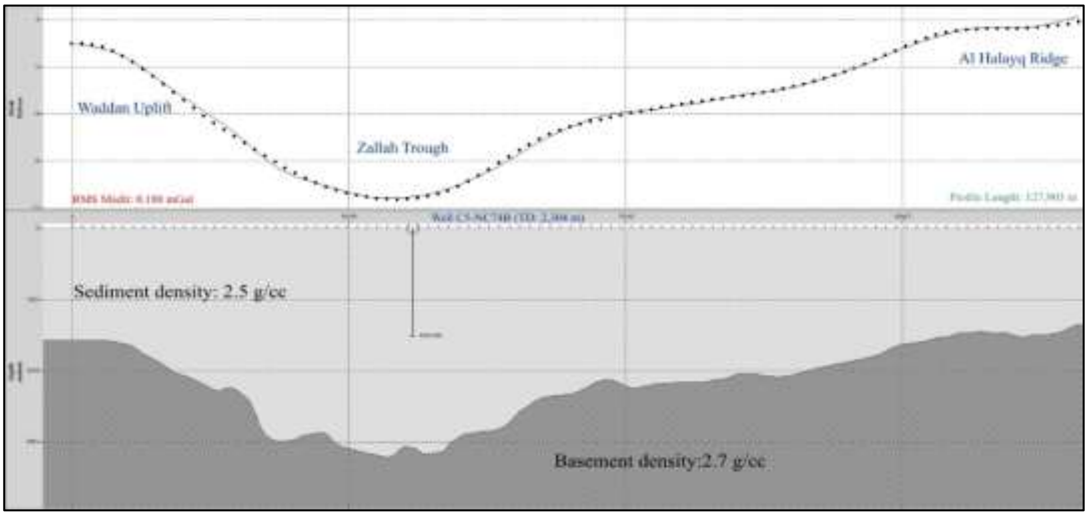

Figure 11b. Two-dimensional forward-modelled geological cross-section along profile WZG-02, from the Waddan Uplift, across the Zallah Trough, to Al Hulayq Ridge, showing the observed and calculated residual gravity curves (RMS = 0.188 mGal), the modelled sediment layer (2.50 g/cm^3) and basement complex (2.7 g/cm^3), and the stepped basement interface. The vertical marker near the profile's deepest point indicates the total depth of well C5-NC74B (TD = 2,304 m; the well does not reach the interpreted basement), shown for reference against the modelled basement depth at this location.

5. DISCUSSION

The convergence of independent lines of evidence in this study — Bouguer and residual anomaly patterns, THG, TDR, and analytic signal edge detection, Euler deconvolution depths, and the density-calibrated forward model along WZG-02 — supports a fault-controlled, internally segmented horst–graben architecture for the Zallah Trough, rather than a single, simple sedimentary sag. The two internal closed minima resolved consistently across the Bouguer, residual, and analytic signal products, separated by a basement saddle, indicate that the trough is compartmentalised into at least two sub-basins, a level of internal structural detail not previously documented for this specific area and one that would benefit from targeted seismic verification.

A sensitivity test using a second-order polynomial trend surface produced nearly identical residual-anomaly patterns, including the locations, amplitudes, and orientations of the principal anomalies. This similarity indicates that the interpreted residual features are robust and are not strongly dependent on the selected polynomial order.

The two marginal faults bounding the trough — corroborated independently by THG, TDR zero-crossings, Euler solution clusters, and, most directly, by the forward-model steps at profile distances of approximately 16,886 m and 61,047 m along WZG-02 — are shown by the Euler depth solutions to deepen systematically from north to south, consistent with both being dipping structures rather than vertical faults. Their convergence at the southern end of the study window, marked by the deepest and most concentrated Euler solution cluster (with depths exceeding 7,000 m and locally more than 8,500 m) and by a near-equant, non-elongate zone of high THG distinct in geometry from the linear marginal trends, is reinterpreted here as a fault-intersection zone. This reinterpretation illustrates the importance of using Euler-derived depth information, rather than plan-view anomaly shape alone, to distinguish structural saddles from zones of fault convergence — an initial, shape-based reading of this zone as a shallow saddle was revised once the corresponding Euler depths were examined.

The apparent difference in basin geometry between the elongate, NW–SE Bouguer expression of the trough and the broader, more equant analytic-signal expression of its deepest part raises the possibility that the basin's bounding structure is not uniform with depth — for example, that fault dip or basin width varies from shallow to deep levels. This is consistent with, though not proven by, the systematic north-to-south deepening of the marginal faults recovered from Euler deconvolution, and is proposed here as a hypothesis for future testing rather than an established conclusion.

The depths obtained from the power-spectrum analysis, Euler deconvolution, and 2D forward modelling represent different aspects of the subsurface sources. The power-spectrum analysis estimates characteristic or average depths for ensembles of sources, Euler solutions provide localized approximate source depths, whereas the forward model estimates a plausible basement geometry along profile WZG-02. Therefore, differences among the three depth estimates are expected and do not necessarily indicate inconsistency.

The forward-modelled depths (maximum 5,050 m, minimum 2,070 m along WZG-02) are shallower than both the power-spectrum deep-source depth (7.62 ± 0.22 km) and the deepest Euler solutions recovered in the fault-intersection zone (>8,500 m). This difference is attributed to the fact that WZG-02 does not cross the deepest, fault-intersection part of the study area, and that the power spectrum yields a window-averaged regional estimate rather than a profile-specific value; the two methods are therefore complementary rather than contradictory, and their comparison illustrates the value of reporting local (profile-based) and regional (spectral) depth estimates alongside one another rather than in isolation.

The largest local misfit along WZG-02 (up to 0.51 mGal, at the profile's southeastern end within Al Hulayq Ridge) could not be linked to any independently mapped lineament, and is attributed provisionally to a basement density within the ridge departing from the uniform 2.7 g/cm³ assumed elsewhere in the model. This is a testable hypothesis: a revised model incorporating a laterally variable basement density, or an independent density constraint from a well located within Al Hulayq Ridge, would help resolve whether this misfit reflects an unmodelled density contrast or an artefact of the EGM2008 model's resolution near the edge of the study window.

The gravity highs over Waddan Uplift, Gattar Ridge, Al Qarqaf Arch, and Al Hulayq Ridge are interpreted as areas of relatively shallow or dense basement, broadly comparable to the horst structure described over the nearby Raguba Field, where a belt of positive Bouguer anomalies was attributed to shallow crystalline basement flanked by negative values over adjacent sediment-filled lows (El-Batroukh & Zentani, 1980). This fault-controlled horst–graben pattern is broadly consistent with the general association between basement-controlled highs, adjoining fault-bounded troughs, and hydrocarbon occurrence documented elsewhere in the western Sirte Basin, where structural traps are commonly related to major fault systems bounding platforms and troughs (Abdunaser, 2015), and with the NW–SE structural grain reported over the Ajdabiya Trough, the Gerad Graben, and the Abu Tumayam Trough (Eshanibli et al., 2021, 2024, 2025; Saheel et al., 2010). This association is presented strictly as a regional and conceptual analogy: gravity data alone cannot demonstrate the presence of a working petroleum system, and any petroleum-system inference from the present analysis should be tested against seismic, well, and geochemical data before any site-specific interpretation is drawn.

6. LIMITATIONS AND FUTURE WORK

- EGM2008 is a global satellite-derived gravity model gridded here at 1000 m spacing; it may not resolve structures narrower than several kilometres, and the high-wavenumber noise floor identified in the power spectrum (beyond ~0.40 cycles per grid unit) sets a practical short-wavelength limit on the interpretation.
- The sediment density of 2.50 g/cm³ used in the forward model was adopted directly from the median RHOB value obtained from well C5-NC74B, selected as the calibration well from among three candidate wells in the Safsaf field (Table 1). The adopted density was held constant with depth as a modelling simplification. Because the well's total depth of 2,304 m is markedly shallower than the modelled basement interface at its location (Figure 11b), the RHOB calibration constrains the sedimentary density but does not directly constrain the deeper basement geometry. Compaction-related density increase and other depth-dependent variations are therefore not represented in the current model and may contribute to the unexplained local misfit within Al Hulayq Ridge.
- Euler deconvolution was performed with a single structural index (N = 0.0); a formal sensitivity test across alternative structural indices was not carried out in this study and is recommended before the depth solutions are used for purposes requiring higher confidence, such as prospect-scale evaluation.
- The two-dimensional forward model is based on a single representative profile (WZG-02); the full three-dimensional basement geometry, and in particular the geometry of the fault-intersection zone identified

at the southern convergence of the two marginal faults, has not been directly modelled and would benefit from additional profiles or a full 3-D inversion.

- The present interpretation requires independent validation by seismic reflection, additional well control (including a well located within Al Hulayq Ridge), and higher-resolution ground or airborne gravity data, particularly to test the hypothesis of internal basin segmentation and depth-dependent fault geometry proposed in Section 5.

7. CONCLUSION

This study presents a multi-method, internally cross-validated gravity interpretation of the basement architecture and probable fault framework of the Zallah Trough and adjacent structural highs in the western Sirte Basin, strictly within the 17°–18° E, 28°–29° N window, using EGM2008 geopotential gravity data at 1000 m grid spacing. The principal mapped structural trend is NW–SE, with subordinate NE–SW and N–S lineaments. The trough is shown to be internally segmented into at least two sub-basins bounded by two marginal, south-dipping faults that converge in a fault-intersection zone at the southern end of the study window. Power-spectrum analysis resolves two well-constrained characteristic depths (7.62 ± 0.22 km and 2.07 ± 0.15 km), and a density-calibrated forward model along profile WZG-02 (RMS = 0.188 mGal) indicates basement depths ranging from 5,050 m beneath the Zallah Trough axis to 2,070 m beneath Al Hulayq Ridge, with the two principal basement steps in the model independently corroborated by tilt-derivative zero-crossings. These results provide a quantitatively constrained regional structural framework intended to guide subsequent seismic and well-constrained studies; the interpretation should be treated as a preferred geological scenario, explicit about its remaining uncertainties (Section 6), rather than as a unique solution.

REFERENCES

Abdunaser, K. M. (2015). Review of the petroleum geology of the western part of the Sirt Basin, Libya. *Journal of African Earth Sciences, 111*, 76–91. https://doi.org/10.1016/j.jafrearsci.2015.07.005

Ahlbrandt, T. S. (2001). *The Sirte Basin Province of Libya—Sirte-Zelten Total Petroleum System*. U.S. Geological Survey Bulletin 2202-F, 29 pp. https://doi.org/10.3133/B2202F

Ambrose, G. J. (2000). The geology and hydrocarbon habitat of the Sarir Sandstone, SE Sirt Basin, Libya. *Journal of Petroleum Geology, 23*(2), 165–192. https://doi.org/10.1111/j.1747-5457.2000.tb00489.x

Anketell, J. M. (1996). Structural history of the Sirt Basin and its relationship to the Sabratah Basin and Cyrenaican Platform, northern Libya. In M. J. Salem, A. S. El-Hawat, & A. M. Sbeta (Eds.), *The Geology of the Sirt Basin* (Vol. 3, pp. 57–89). Amsterdam: Elsevier.

Blakely, R. J. (1996). *Potential Theory in Gravity and Magnetic Applications*. Cambridge: Cambridge University Press. https://doi.org/10.1017/CBO9780511549816

El-Batroukh, S. I., & Zentani, A. S. (1980). Gravity interpretation of Raguba Field, Sirte Basin, Libya. *Geophysics, 45*(7), 1153–1163. https://doi.org/10.1190/1.1441114

Eshanibli, A., Khalil, A. E., Younis, A., & Ghanoush, H. (2020). Structural framework of the Zelten Platform, South Sirte Basin, Libya using potential fields modelling. Acta Geodynamica et Geomaterialia, 17(2), 229–236. https://doi.org/10.13168/AGG.2020.0017

Eshanibli, A. S., Osagie, A. U., Ismail, N. A., & Ghanush, H. B. (2021). Analysis of gravity and aeromagnetic data to determine structural trend and basement depth beneath the Ajdabiya Trough in northeastern Libya. *SN Applied Sciences, 3*, Article 228. https://doi.org/10.1007/s42452-021-04263-7

Eshanibli, A., Ismail, N. A., Dugdug, A., Ghanush, H. B., & Buazza, A. (2024). Integrated analysis on gravity, 2D seismic, and well data of the Abu Tumayam Trough, western Sirt Basin, Libya. *Acta Geodynamica et Geomaterialia, 21*(2), 139–150. https://doi.org/10.13168/AGG.2024.0013

Eshanibli, A., Ismail, N. A., Ghanush, H. B., Dugdug, A., Uyimwen, O. A., Khalifa, N., et al. (2025). Delineation of depth to basement and subsurface structures beneath the Gerad Graben, western Sirt Basin, Libya, from gravity and aeromagnetic data. *Energy Geoscience, 6*(4), Article 100468. https://doi.org/10.1016/j.engeos.2025.100468

Eshaghzadeh, A. (2015). Image edge detection of the total horizontal gradient of gravity data using the normalized tilt angle. *Geodynamics Research International Bulletin, 3*(4), XXVIII–XXXIII.

Goudarzi, G. H. (1980). Structure—Libya. In M. J. Salem & M. T. Busrewil (Eds.), *The Geology of Libya: Second Symposium on the Geology of Libya* (Vol. 3, pp. 879–892). London: Academic Press.

Miller, H. G., & Singh, V. (1994). Potential field tilt—a new concept for location of potential field sources. *Journal of Applied Geophysics, 32*(2–3), 213–217. https://doi.org/10.1016/0926-9851%2894%2990022-1

Omran, O. E. O., & Elosta, H. N. R. (2024). Magnetic interpretation of Zaggut Oil Field, Sirt Basin—Libya. *Almarifa Journal of Humanities and Applied Sciences, 2*(1). Available at: https://journal.almarifa.edu.ly/index.php/ar/article/view/125

Reid, A. B., Allsop, J. M., Granser, H., Millett, A. J., & Somerton, I. W. (1990). Magnetic interpretation in three dimensions using Euler deconvolution. *Geophysics, 55*(1), 80–91. https://doi.org/10.1190/1.1442774

Saheel, A. S., Samsudin, A. R., & Hamzah, U. (2010). Interpretation of the gravity and magnetic anomalies of the Ajdabiya Trough in the Sirt Basin, Libya. *European Journal of Scientific Research, 43*(3), 316–330.

Verduzco, B., Fairhead, J. D., Green, C. M., & MacKenzie, C. (2004). New insights into magnetic derivatives for structural mapping. *The Leading Edge, 23*(2), 116–119. https://doi.org/10.1190/1.1651454